HHS Public Access

Author manuscript

Biomed Mater. Author manuscript; available in PMC 2015 June 05.

Published in final edited form as:

Biomed Mater. 2014 February ; 9(1): 011002. doi:10.1088/1748-6041/9/1/011002.

Microablation of collagen-based substrates for soft tissue engineering

Vivek A. Kumar[1,2,3], **Adam W. Martinez**[3], **Jeffrey M. Caves**[1,2], **Nisarga Naik**[1,2], **Carolyn A. Haller**[1,2], and **Elliot L. Chaikof**[1,2,3]

Elliot L. Chaikof: echaikof@bidmc.harvard.edu

[1]Department of Surgery, Beth Israel Deaconess Medical Center, Harvard Medical School, Boston, MA 02215

[2]Wyss Institute of Biologically Inspired Engineering of Harvard University, Boston, MA 02215

[3]Department of Biomedical Engineering, Georgia Institute of Technology/Emory University, Atlanta, GA 30332

Abstract

Noting the abundance and importance of collagen as a biomaterial, we have developed a facile method for the production of dense fibrillar extracellular matrix mimicking collagen-elastin hybrids with tunable mechanical properties. Through the use of excimer laser technology, we have optimized conditions for the ablation of collagen lamellae without denaturation of protein, maintenance of fibrillar ultrastructure and preservation of native D-periodicity. Strengths of collagen-elastin hybrids ranged from 0.6 - 13 MPa, elongation at break from 9 - 70 %, and stiffness from 2.9 - 94 MPa, allowing for the design of a wide variety of tissue specific scaffolds. Further, large (centimeter scale) lamellae can be fabricated and embedded with recombinant elastin to generate collagen-elastin hybrids. Exposed collagen in hybrids act as cell adhesive sites for rat mesenchymal stem cells that conform to ablate waveforms. The ability to modulate these features allows for the generation of a class of biopolymers that can architecturally and physiologically replicate native tissue.

Keywords

Tissue engineering; excimer laser; mesenchymal stem cells; collagen; elastin

1. Introduction

Tissue engineering has attempted to address the need for advanced materials to recapitulate native tissue in structure, function and interact favorably with the host [1, 2]. Biosynthetic materials and biologically derived materials have been investigated with much interest to provide a native tissue mimetic platform for the development of artificial tissues and organs. Current limitations of reconstituted biosynthetic materials include the lack of tailorability for specific tissues and the small range of applications each material can be designed for.

The authors have no conflicts of interest to disclose.

Critically for collagen based substrates, current technologies have focused on relatively weak hydrogel systems that fail to match significantly stronger soft and hard tissues – lacking critical strength, stiffness and elongation characteristics [3].

There has been a focus on the development of fabrication techniques that aim to enhance biosynthetic material properties to mimic native tissue [4, 5]. Processing of collagen into scaffolds for tissue engineering has focused on hydrogels, electrospinning or hybrid technologies [6]. These techniques yield matrices that are either unable to withstand physiologic mechanical loading or have non-biomimetic denatured collagen sequences [4, 6–8]. Recently published data from other groups and our own have shown the ability to modulate mechanical strength of collagen by processing into dense collagen fiber bundles [7, 9]. We have built upon this and propose a rapid fabrication technique for the development of large centimeter scale micron thin collagen fabrics. We have recently described a recombinant elastin-like protein polymer (ELP) which has been shown to be biocompatible [10–12], tailorable [13, 14] and mechanically resilient [10, 15–17]. We have demonstrated utility of elastin either alone or in combination with collagen mats for vascular and musculo-fascial applications, with mechanical studies outlining contributions of each polymeric substituent [11, 18–22]. We have furthered these technologies by attempting to mimic the crimped form of fibrous collagen, which supports tensile loading in native tissue (10 - 200 μm wavelengths) [23, 24]. To do this, we have applied excimer laser ablation to create “wavy” collagen structures that enhance tissue engineered matrix compliance (<10 - 60 % elongation at break) with no appreciable protein denaturation. Collagen-elastin hybrids show a wide range of tunable mechanics: strengths of 0.5 - 13 MPa, elongation at break of 9 - 70 %, and stiffness of 3 - 94 MPa mimicking a wide range of native soft tissue. Cytocompatibility was established by culture of bone marrow derived mesenchymal stem cells, showing confluence within hours and conformal scaffold based cell morphology. Through the development and utilization of layer-reinforced collagen networks and microfabrication techniques, we have developed a natural biopolymer matrix with tunable mechanical properties that have potential for use as biosynthetic blood vessels, tendon replacements, hernia patches, muscle tissue, nerve guidance conduits, artificial skin and other soft tissue applications [8, 19, 25, 26].

2. Materials and methods

Isolation and purification of monomeric collagen

Monomeric Type I rat tail tendon collagen was obtained by acid extraction from Sprague-Dawley rats (Pel-Freez Biologicals, Rogers, AR) following a procedure adapted from Silver and Trelstad [27]. Briefly, rat tail tendons were extracted and dissolved in 10 mM HCl for 4 h at 25°C, centrifuged at 30,000g at 4°C for 30 mins and vacuum filtered (20 μm, 0.45 μm and 0.2 μm filters). Collagen in HCl was precipitated from solution by adding NaCl (0.7 M final), centrifuged, redissolved in 10 mM HCl and dialyzed against 20 mM phosphate buffer, 10 mM HCl at 4°C and deionized water at 4°C. The collagen was then frozen and lyophilized till use.

Production of collagen lamellae

Collagen lamellae were generated as described elsewhere [19]. Briefly, monomeric rat tail tendon collagen dissolved in 10 mM HCl was neutralized using a gelation buffer (4.14 mg/mL monobasic sodium phosphate, 12.1 mg/mL dibasic sodium phosphate, 6.86 mg/mL TES (N-tris (hydroxymethyl) methyl-2-aminoethane sulfonic acid sodium salt, 7.89 mg/mL sodium chloride, pH 8.0) at 4°C, in rectangular molds (10 × 7.0 cm) for 24 h. Gel thicknesses were 4 mm. Gels were subsequently placed in a fiber incubation buffer (7.89 mg/mL sodium chloride, 4.26 mg/mL dibasic sodium phosphate, 10 mM Tris, pH 7.4) at 37°C for 48 h to promote fibrillogenesis [28]. Gels were rinsed in deionized water and dried at room temperature to create collagen mats. Serial dehydration of gels atop mats created multilammelar constructs. Mats were crosslinked in genipin at 6 mg/mL in 1x PBS at 37°C for 24 h.

Excimer ablation of collagen lamellae

Two mask designs were used in this study: linear and sawtooth (wavy) quartz masks. Quartz contact masks (Advance Reproductions, MA) were fabricated using photolithography and wet etching of 5 μm thick aluminum coated quartz. For the linear design, the wave strip length was 2 mm, wave strip width was 120 μm, interstrip width 10 μm, and vertical strip thickness 100 μm. For the sawtooth (wavy) waveform, the wave strip length was 1 mm, wave strip width 60 μm, interstrip width 60 μm, angle of the wave crest 60°, and vertical strip thickness of 100 μm. Design nomenclature is illustrated in Figure 2A. The mask was placed over collagen mats and ablated with an excimer laser with parameters adjusted to yield a fluence of 26.7 J/cm^2 (Microelectronics Research Center at Georgia Tech, Atlanta, GA).

Microdifferential scanning calorimetry of collagen lamellae

Thermal denaturation temperature and enthalpy of denaturation were measured using differential scanning calorimeter (μDSC, SETARAM, Pleasanton, CA). A total of 5 - 10 mg of lyophilized collagen, dried collagen lamellae pre or post excimer ablation, and after crosslinking in genipin were hydrated in 0.5 mL of PBS for 10 h at 5°C. Lamellae were then heated from 5°C to 90°C and cooled to 5°C at 0.5°C/min. The enthalpy of denaturation, H_D, and denaturation temperature, T_D, were measured and complete denaturation confirmed by the lack of a denaturation peak upon repeated heating to 90°C and cooling.

Synthesis of a recombinant elastin-like protein polymer (ELP)

Development and production of the ELP, LysB10, has been described elsewhere [10]. Briefly, a triblock amphiphilic copolymer was designed to contain hydrophobic endblocks and a hydrophilic midblock. The 75 kDa polypeptide comprised 33 repeats of the pentapeptide sequence $[IPAVG]_5$, and the 58 kDa midblock comprised 28 repeats of the sequence $[(VPGAG)_2VPGEG(VPGAG)_2]$. Flanking both the hydrophobic plastic endblocks and the hydrophilic elastic midblock were the crosslinkable amino acid sequences [KAAK], which allow for amine-based crosslinking. Subsequent to expression in *E. coli*, protein was extracted and purified using hot/cold centrifugation cycles and nucleic acid removal. Protein solutions were then dialyzed against water and lyophilized.

Fabrication of planar nanofibrous collagen-elastin hybrids

LysB10, dissolved in molecular grade water (10 mg/mL, 4°C) was used to embed collagen lamellae in a sandwich molding setup. The setup was warmed to 25°C to allow the LysB10 solution to gel, creating collagen-elastin hybrids [19, 22].

Imaging of hybrid architecture

Optical microscopy, fluorescence microscopy, scanning electron microscopy (SEM), and transmission electron microscopy (TEM) were used to analyze the collagen structure. For SEM studies, dry collagen lamellae were hydrated in water for 24 h and dehydrated in serial exchanges of ethanol-water mixtures from 30 % - 100 %, critical point dried (Auto Samdri 815 Series A, Tousimis, Rockville, MD), sputter coated with 8 nm of gold (208HR Cressington, Watford, England) and imaged at an accelerating voltage of 10 keV using a field emission scanning electron microscope (Zeiss Supra 55 FE-SEM, Peabody, MA). For TEM studies, samples in PBS were washed in 0.1 M cacodylate buffer and fixed in glutaraldehyde, partially dehydrated in ethanol and stained with uranyl acetate. Samples were then fully dehydrated in ethanol, embedded in resin, polymerized and sections cut (60 - 80 nm) using a RMC MT-7000 ultramicrotome (Boeckeler, Tucson, AZ). Post-staining with uranyl acetate and lead citrate was followed by imaging using a JOEL JEM-1400 TEM (JOEL, Tokyo, Japan) at 90 keV.

Rat mesenchymal stem cell (rMSC) cell culture

Bone marrow-derived rMSCs (courtesy of Steven Stice, University of Georgia, GA) were seeded onto collagen-elastin hybrid constructs to establish cytocompatibility. Hybrid scaffolds with and without microablation were sterilized in 70 % ethanol for 30 min, washed several times in 1X PBS, and incubated in media for 30 min prior to cell seeding. Cells were cultured in Alpha MEM, supplemented with 10 % fetal bovine serum, 1 % L-glutamine and 1 % penicillin-streptomycin. Cells were removed from tissue culture-treated polystyrene flasks using 0.25 % trypsin-EDTA, suspended in media, and seeded at a concentration of 100,000 cells/cm^2 for 24 h.

Assessment of cellular viability and organization

For Live/Dead staining, scaffolds were incubated with 2 mL of Live/Dead stain (Invitrogen, Carlsbad, CA), and imaged using a Leica SP5 confocal (Leica, Buffalo Grove, IL). For cellular actin filament organization, scaffolds were fixed, stained with Alexa Fluor 568, counterstained with DAPI Prolong Gold™ (Invitrogen, Carlsbad, CA) and imaged after 24 h using confocal microscopy.

Mechanical testing of hybrids

Collagen-elastin hybrid sheets, with or without microablation, were cut into 20 mm x 5 mm strips and mounted onto a Dynamic Mechanical Thermal Analyzer V (Rheometric Scientific, Piscataway, NJ) with a gauge length of 10 mm, immersed in PBS at 37°C. Samples were preconditioned 15 times to 66 % of the average maximum failure strain determined from pilot samples, and then tested to failure at 5 mm/min (n = 8 for each group). Hydrated thickness was measured using optical microscopy for calculation of cross-

sectional area. Young's modulus was determined from the slope of the last 4 % of the stress-strain curve.

Statistical Analysis

Means and S.D. were obtained for all measurements, image analyses and mechanical data. Comparisons were made using the Student's *t* test for paired data, ANOVA for multiple comparisons, and Tukey post hoc analysis for parametric data. Nonparametric tests were carried out using the Kruskal-Wallis ANOVA, with Dunn's post hoc analysis as indicated. Values of $p < 0.05$ were considered statistically significant.

3. Results and Discussion

3.1 Generation of collagen lamellae and nanofibrous hybrids

Recapitulation of the nanofibrous structure is important to the development of scaffolds for tissue engineering. Several technologies aim to mimic this by electrospinning [29, 30], utilizing nanofibrous scaffolds [31] and using biological naturally derived or reconstituted matrices [32]. However several drawbacks, such as potential acidic by-products of degradation or non-natural monomers, immune rejection, lack of mechanical tunability or loss of native structure of reconstituted biological polymers may cause adverse responses in vivo [2–4, 18, 30]. We have consequently chosen to use reconstituted collagen materials with high strength and tunable mechanical properties that are processed to maintain native structure, and fabricated to yield mechanical and structural anisotropy. To fill the ablated portions of the collagen, we have used a synthetic elastin mimetic triblock hydrogel developed by our lab, Lys-B10 [10]. The hydrophobic (Ile-Pro-Ala-Val-Gly) block, flank a central hydrophilic midblock (Val-Pro-Gly-Glu-Gly) that aids in coordination of water molecules in aqueous solutions. However, above the lower critical solution temperature or inverse transition temperature the hydrophobic endblocks coaccervate, yielding a hydrogel. We have shown the ability to introduce crosslinkable moieties into the elastin structure to promote intra/inter molecular crosslinking, as well as crosslinking to other protein based materials through the aid of labile lysine residues [10, 13–15]. We have demonstrated that these elastin mimetics resist thrombosis and can be used for soft tissue repair and replacement [11, 12, 18, 19, 21, 22]. We used a temperature controlled sandwich molding technique to infuse Lys-B10 into collagen lamellae, leading to nanofibrous collagen-elastin hybrids, schematically shown in Figure 1 [20–22]. Dry mats before and after the addition of Lys-B10 had spatial densities of 0.77 ± 0.06 mg/cm^2 or 0.98 ± 0.05 mg/cm^2, respectively, suggesting the collagen-elastin hybrids are 78.5 % collagen and 21.5 % ELP by dry weight.

3.2 Preservation of collagen macromolecular structure after ablation

Ultraviolet lasers have been used in a variety of applications in medicine including treatment of psoriasis [33], ophthalmologic applications [34], arthroscopy [35], laser-assisted vascular plaque ablation [36], and development of tissue engineering scaffolds [37–41]. One of the most established examples of excimer laser ablation is in laser-assisted in situ keratomileusis (LASIK) eye surgery. Unlike thermal ablation, which is the basis for CO_2 laser ablation, the benefit of excimer laser ablation is that it excites the molecular bonds sufficiently to dissociate and ablate them, without thermal decomposition to elemental compounds.

Further, the dissociated molecular products are cleared by an airstream, which leaves "clean" and non-denatured substrata that maintains native phenotype. Although non-thermal in nature, excimer laser ablation and other UV based optical ablation schemes generate small amounts of localized heat when maintained on a specific locus. Specific to tissue engineering, Nakayama and Matsuda used an excimer laser to improve compliance of polyurethane tubes by microablation of holes of a variety of sizes [41]. Engelmayr and colleagues used a similar approach to ablate adjacent holes in a polyglycerol sebacate scaffold. The resulting scaffold had an accordion-like honeycomb architecture with enhanced compliance and appreciable cellular alignment [39]. Further, Chollet et al. report the use of excimer laser ablation to modulate cellular alignment. Specifically they report that 25 μm to 100 μm width RGD patterned substrates (separated by laser ablation) result in cellular alignment [38]. Another important factor influencing laser residence time is ablation mode – direct-write or rastering over a mask. The former is typically more time intensive and involves "writing" a pattern of individual features on the substrate. The latter, however, involves moving a relatively larger laser spot across the substrate. When coupled with a mask that is laser opaque, features, as determined by the mask, are ablated. Although the theoretical resolution of excimer laser ablation is the wavelength of the beam (in our studies, 248 nm), the practical resolution is typically 1 order of magnitude higher – 2 - 10 μm. We have thus generated aluminum-on-quartz masks that attenuate UV light, but allow transmission in 2 - 10 μm or greater gaps (features). Consequently, we have been able to rapidly fabricate detailed patterns on protein-based matrices with high fidelity as demonstrated in Figures 2 and 4. To determine the optimal conditions that result in collagen ablation without denaturation, parameters such as fluence (spatial laser energy density) and rastering rate ensured collagen mats were ablated with minimal denaturation. Thermal denaturation was determined by analyzing thermal transitions of collagen, which showed no measurable denaturation, and analyzing collagen ultrastructure by noting the retention of bulk and ablation edge native collagen D-periodic 67 nm banding patterns and fibrillar structure. These results are similar to those reported in clinical practice with excimer laser ablation strategies yielding small (0.1 - 0.3 μm) regions of damage [42]. Thermal analysis showed that the denaturation temperature of lyophilized collagen was lower than uncrosslinked and crosslinked collagen lamellae, 46.0 ± 0.5°C, 52.9 ± 0.4°C and 73.2 ± 2.1°C, respectively (Table 1). Changes in ultrastructure conferred during phosphate buffer treatment and densification of the matrix during lamella fabrication contribute to a higher T_D for collagen mats than lyophilized collagen. Lyophilized collagen and collagen lamellae exhibited similar H_D. Crosslinking of matrices resulted in a greater stabilization of the collagen structure and consequently raises T_D, but lowers H_D (Table 1). There was no significant difference in the thermal transitions or enthalpy between collagen lamellae with and without ablation, suggesting no measurable loss in triple helical structure (Figure 3, Table 1).

3.3 Design of mechanically variant structures for optimized mechanical compliance

Pilot designs ablated into collagen lamellae to demonstrate proof of principle and benchmark ablation techniques involved ablation of holes 10 - 100 μm in diameter (data not shown), direct write of lines and waves, and variations of waveform designs (Figure 2A). However, it was recognized that the strip width to height (film thickness) ratio needed to be

< 1 to ensure features were stable and did not collapse laterally during subsequent processing. Linear ablation patterns were also generated to determine the altered mechanical response as a function of excimer laser ablation pattern. Wave patterns with varied vertical strip thickness of 100 μm and interstrip thickness of 10 μm, demonstrated the modulation of mechanical strength as a function of patterning. Aluminum coated quartz allowed laser transmission through 10 μm gaps, showing high ablation fidelity, with patterns on the centimeter scale to be completely ablated over a period of less than 1 h (Figure 2A, Figure 4A, C). Collagen wave ablation showed high precision and uniformity under optical microscopy (Figure 4B, D), with a nanofibrous (80 μm) fibrillar matrix assessed via SEM (Figure 4E, F). Preservation of native collagen structure, indicated by D-periodic banding was noted in the matrix bulk (Figure 4G), and edges of waves (Figure 4H). The utility of excimer laser ablation to modulate stiffness and extensibility is shown in Figure 5. Linear ablation patterns resulted in a greater than 50 % reduction in tensile strength from unablated mats (4.01 ± 0.64 MPa vs. 9.51 ± 1.51 MPa, $p < 0.05$, Figure 5A), while triangular waveform ablation patterns lead to further reduction in mechanical strength (0.98 ± 0.11 MPa). The decrease in strength for ablated constructs may be due to microdefects post-ablation that act as points of stress concentration and a decreased volume fraction of primarily load bearing collagen for triangular waveform patterns as compared to linear patterns (62.8 ± 3.5 % vs 85.2 ± 8.4 %, $n = 8$, $p < 0.05$). Likewise, strain at failure increased from 9.43 ± 2.76 % for linear ablation patterns to 69.5 ± 10.9 % for triangular waveform patterns. Calculated extension based on length of equilateral triangular wavy waveform suggests a theoretical strain at failure of 100 %. However, thicker non-linear aspect ratios arise at wave peaks and troughs, which may result in out of plane bending of mats reducing linear strain response, and potential twisting during straightening of collagen strips (Figure 2). Further, planar unablated (vertical strip) regions, which cover 100 μm every 2 mm of waveform, yield strains similar to unablated constructs (Figure 2, 4). Unablated constructs did not have a significantly different strain at failure from linear ablated constructs (12.4 ± 1.96 %, Figure 5B). The Young's modulus of unablated and linear ablated constructs were not significantly different (93.7 ± 19.8 MPa vs. 88.1 ± 12.9 MPa), but were higher than that of wavy triangular wave patterned collagen (5.06 ± 1.34 MPa, $p < 0.05$). Together these results suggest the ability to generate a series of mechanically tunable collagen based constructs that have strengths and stiffnesses that mimic soft tissues, such as cartilage [26], ligament [8, 26], coronary artery [8], and carotid artery [25] (Table 2).

3.5 Structural features dictate cellular adhesion

To establish the cytocompatibility of hybrids and their potential applicability in developing tissue engineered constructs, we have assessed adhesion and spreading of commonly used rat bone marrow derived mesenchymal stem cells, rMSCs, on microablated collagen-elastin hybrids. While collagen is well known to be highly cell adhesive, we have previously shown that elastin mimetic gels have enhanced cell adhesion when modified with cell binding sequences such as fibronectin, RGD or CCN1 [13, 14, 43]. To demonstrate the preservation of cell adhesivity on collagen-elastin hybrids, scaffolds were seeded with rMSCs and observed for adhesion at 4 h and proliferation at 24 h, at a seeding density of 100,000 cells/cm^2 (Figure 6A). Wavy ablated matrices showed conforming of cells discretely to waveform patterns, as seen in Live/Dead staining and staining of cytoskeletal actin filaments

(Figure 6B, C), without cell adhesion on elastin mimetic, Lys-B10, in lamellae gaps. The purpose of this cell adhesion study was to show preservation of cell adhesivity on collagen exposed regions of hybrids. Future studies will evaluate longer timepoints in specific applications with specific cells. In vivo studies in a similar collagen-elastin hybrid system used for cardiovascular tissue engineering or musculo-fascial repair have demonstrated infiltration of scaffolds with cells, a muted inflammatory response, and wound healing [18, 19]. Several studies have noted the importance of cells in recapitulation of native tissue structure and function. For example, SMC in the vascular media act to both maintain contractility during pulsatile blood flow, as well as vasoconstrict as a function of neuronal or chemokine action. Further, cells in the myocardium and other muscle tissue align in the direction of physiologic stress to aid in biomechanical function and contractility. For tissue-engineered constructs, development of a cellular niche that complements cell adhesion, and proliferation is quintessential to promotion of engrafted material healing and integration. The ability to conform cells in vitro, however, has been attempted using a myriad of techniques [44]. Engelmayr et al. have demonstrated that cells seeded in micron-sized pores created in polyglycerol sebacate result in localized cardiomyocyte conformity [39]. In contrast to this approach, which uses geometric confinement to conform cells to specific material patterns, an excimer–laser assisted ablation scheme can potentially create ordered micro-ribbons that are intrinsically cell adhesive. Cells appear to conform to the waveform pattern, allowing for rapid generation of large-scale tissue engineered substrates with structurally defined regions for cellular adhesion. An advantage of this approach is the ability to avoid the need for incorporation of additional cell-binding components, such as fibronectin, vitronectin, or related integrin binding peptides.

4. Conclusions

Engineering of substrates for tissue repair and replacement continues to advance. The benefits of collagen are numerous, including its high species homology, ease of availability, intrinsic cell adhesiveness, strength, FDA approval, and ability for large scale fabrication and processing into constructs that are relevant for tissue engineering. This is the first report of the use of excimer laser technology for the ablation of biologically derived protein based matrices suitable for tissue engineering. Through the use of excimer laser technology, we have determined optimal parameters for the ablation of collagen mats with high fidelity and preservation of native structure - determined by differential scanning calirometery, as well as by scanning and transmission electron microscopy. Further, with the addition of recombinantly expressed elastin mimetic proteins, nanofibrous hybrid ECM mimetics have been created. Mechanical testing of ablated collagen-elastin hybrids shows the ability to further modulate mechanical properties including compliance, stiffness and strength to better mimic soft tissue, as well as to coordinate the adhesion of rMSCs. Preferential alignment of cells in the direction of collagen waves provides an additional means to tailor cellular anisotropy.

Acknowledgments

This work was supported by grants from the National Institute of Health: R01HL083867, R01HL60464, and R01HL71336. Electron microscopy was performed at the Center for Nanoscale Systems at Harvard University, and the Wyss Institute of Biologically Inspired Design.

References

1. Vacanti JP, Langer R. Tissue engineering: the design and fabrication of living replacement devices for surgical reconstruction and transplantation. Lancet. 1999; 354(Suppl 1):SI32–34. [PubMed: 10437854]
2. Langer R, Tirrell DA. Designing materials for biology and medicine. Nature. 2004; 428:487–492. [PubMed: 15057821]
3. Lee CH, Singla A, Lee Y. Biomedical applications of collagen. Int J Pharm. 2001; 221:1–22. [PubMed: 11397563]
4. Cen L, Liu W, Cui L, Zhang W, Cao Y. Collagen tissue engineering: development of novel biomaterials and applications. Pediatr Res. 2008; 63:492–496. [PubMed: 18427293]
5. Smith LA, Ma PX. Nano-fibrous scaffolds for tissue engineering. Colloids Surf B Biointerfaces. 2004; 39:125–131. [PubMed: 15556341]
6. Zhang YZ, Su B, Venugopal J, Ramakrishna S, Lim CT. Biomimetic and bioactive nanofibrous scaffolds from electrospun composite nanofibers. Int J Nanomedicine. 2007; 2:623–638. [PubMed: 18203429]
7. Caves JM, Kumar VA, Wen J, Cui W, Martinez A, Apkarian R, et al. Fibrillogenesis in continuously spun synthetic collagen fiber. J Biomed Mater Res B Appl Biomater. 2010; 93:24–38. [PubMed: 20024969]
8. Zhang R, Ma PX. Synthetic nano-fibrillar extracellular matrices with predesigned macroporous architectures. J Biomed Mater Res. 2000; 52:430–438. [PubMed: 10951385]
9. Wang MC, Pins GD, Silver FH. Collagen fibres with improved strength for the repair of soft tissue injuries. Biomaterials. 1994; 15:507–512. [PubMed: 7918903]
10. Sallach RE, Cui W, Wen J, Martinez A, Conticello VP, Chaikof EL. Elastin-mimetic protein polymers capable of physical and chemical crosslinking. Biomaterials. 2009; 30:409–422. [PubMed: 18954902]
11. Sallach RE, Cui W, Balderrama F, Martinez AW, Wen J, Haller CA, et al. Long-term biostability of self-assembling protein polymers in the absence of covalent crosslinking. Biomaterials. 2010; 31:779–791. [PubMed: 19854505]
12. Jordan SW, Haller CA, Sallach RE, Apkarian RP, Hanson SR, Chaikof EL. The effect of a recombinant elastin-mimetic coating of an ePTFE prosthesis on acute thrombogenicity in a baboon arteriovenous shunt. Biomaterials. 2007; 28:1191–1197. [PubMed: 17087991]
13. Ravi S, Krishnamurthy VR, Caves JM, Haller CA, Chaikof EL. Maleimide-thiol coupling of a bioactive peptide to an elastin-like protein polymer. Acta Biomater. 2012; 8:627–635. [PubMed: 22061108]
14. Ravi S, Caves JM, Martinez AW, Haller CA, Chaikof EL. Incorporation of fibronectin to enhance cytocompatibility in multilayer elastin-like protein scaffolds for tissue engineering. J Biomed Mater Res A. 2013; 101:1915–1925. [PubMed: 23225639]
15. Sallach RE, Leisen J, Caves JM, Fotovich E, Apkarian RP, Conticello VP, et al. A permanent change in protein mechanical responses can be produced by thermally-induced microdomain mixing. J Biomater Sci Polym Ed. 2009; 20:1629–1644. [PubMed: 19619402]
16. Wu X, Sallach RE, Caves JM, Conticello VP, Chaikof EL. Deformation responses of a physically cross-linked high molecular weight elastin-like protein polymer. Biomacromolecules. 2008; 9:1787–1794. [PubMed: 18558738]
17. Wu X, Sallach R, Haller CA, Caves JA, Nagapudi K, Conticello VP, et al. Alterations in physical cross-linking modulate mechanical properties of two-phase protein polymer networks. Biomacromolecules. 2005; 6:3037–3044. [PubMed: 16283724]
18. Kumar VA, Caves JM, Haller CA, Dai E, Liu L, Grainger S, et al. Collagen-based substrates with tunable strength for soft tissue engineering. Biomaterials Science. 2013; 1:1193–1202.
19. Kumar VA, Caves JM, Haller CA, Dai E, Liu L, Grainger S, et al. Acellular vascular grafts generated from collagen and elastin analogs. Acta Biomater. 2013
20. Caves JM, Kumar VA, Xu W, Naik N, Allen MG, Chaikof EL. Microcrimped collagen fiber-elastin composites. Adv Mater. 2010; 22:2041–2044. [PubMed: 20544890]

21. Caves JM, Kumar VA, Martinez AW, Kim J, Ripberger CM, Haller CA, et al. The use of microfiber composites of elastin-like protein matrix reinforced with synthetic collagen in the design of vascular grafts. Biomaterials. 2010; 31:7175–7182. [PubMed: 20584549]
22. Caves JM, Cui W, Wen J, Kumar VA, Haller CA, Chaikof EL. Elastin-like protein matrix reinforced with collagen microfibers for soft tissue repair. Biomaterials. 2011; 32:5371–5379. [PubMed: 21550111]
23. Tang H, Buehler MJ, Moran B. A constitutive model of soft tissue: from nanoscale collagen to tissue continuum. Ann Biomed Eng. 2009; 37:1117–1130. [PubMed: 19353270]
24. Elbischger PJ, Bischof H, Holzapfel GA, Regitnig P. Computer vision analysis of collagen fiber bundles in the adventitia of human blood vessels. Stud Health Technol Inform. 2005; 113:97–129. [PubMed: 15923739]
25. Kurane A, Simionescu DT, Vyavahare NR. In vivo cellular repopulation of tubular elastin scaffolds mediated by basic fibroblast growth factor. Biomaterials. 2007; 28:2830–2838. [PubMed: 17368531]
26. Yang S, Leong KF, Du Z, Chua CK. The design of scaffolds for use in tissue engineering. Part I. Traditional factors. Tissue Eng. 2001; 7:679–689. [PubMed: 11749726]
27. Silver FH, Trelstad RL. Type I collagen in solution. Structure and properties of fibril fragments. J Biol Chem. 1980; 255:9427–9433. [PubMed: 7410433]
28. Pins GD, Christiansen DL, Patel R, Silver FH. Self-assembly of collagen fibers. Influence of fibrillar alignment and decorin on mechanical properties. Biophys J. 1997; 73:2164–2172. [PubMed: 9336212]
29. Bhardwaj N, Kundu SC. Electrospinning: a fascinating fiber fabrication technique. Biotechnol Adv. 2010; 28:325–347. [PubMed: 20100560]
30. Dahlin RL, Kasper FK, Mikos AG. Polymeric nanofibers in tissue engineering. Tissue Eng Part B Rev. 2011; 17:349–364. [PubMed: 21699434]
31. Webb AR, Yang J, Ameer GA. Biodegradable polyester elastomers in tissue engineering. Expert Opin Biol Ther. 2004; 4:801–812. [PubMed: 15174963]
32. Hoshiba T, Lu H, Kawazoe N, Chen G. Decellularized matrices for tissue engineering. Expert Opin Biol Ther. 2010; 10:1717–1728. [PubMed: 21058932]
33. Lapolla W, Yentzer BA, Bagel J, Halvorson CR, Feldman SR. A review of phototherapy protocols for psoriasis treatment. J Am Acad Dermatol. 2011; 64:936–949. [PubMed: 21429620]
34. Krueger RR, Rabinowitz YS, Binder PS. The 25th anniversary of excimer lasers in refractive surgery: historical review. J Refract Surg. 2010; 26:749–760. [PubMed: 20954683]
35. Glossop ND, Jackson RW, Koort HJ, Reed SC, Randle JA. The excimer laser in orthopaedics. Clin Orthop Relat Res. 1995:72–81. [PubMed: 7641463]
36. Litvack F, Grundfest WS, Papaioannou T, Mohr FW, Jakubowski AT, Forrester JS. Role of laser and thermal ablation devices in the treatment of vascular diseases. Am J Cardiol. 1988; 61:81G–86G.
37. Tandon N, Marsano A, Maidhof R, Numata K, Montouri-Sorrentino C, Cannizzaro C, et al. Surface-patterned electrode bioreactor for electrical stimulation. Lab Chip. 2010; 10:692–700. [PubMed: 20221556]
38. Chollet C, Lazare S, Guillemot F, Durrieu MC. Impact of RGD micro-patterns on cell adhesion. Colloids Surf B Biointerfaces. 2010; 75:107–114. [PubMed: 19775874]
39. Engelmayr GC Jr, Cheng M, Bettinger CJ, Borenstein JT, Langer R, Freed LE. Accordion-like honeycombs for tissue engineering of cardiac anisotropy. Nat Mater. 2008; 7:1003–1010. [PubMed: 18978786]
40. Matsuda T, Chung DJ. Microfabricated surface designs for cell culture and diagnosis. ASAIO J. 1994; 40:M594–597. [PubMed: 8555584]
41. Nakayama Y, Matsuda T. Microporous polymer surfaces prepared by an excimer laser ablation technique. ASAIO J. 1994; 40:M590–593. [PubMed: 8555583]
42. Puliafito CA, Steinert RF, Deutsch TF, Hillenkamp F, Dehm EJ, Adler CM. Excimer laser ablation of the cornea and lens. Experimental studies. Ophthalmology. 1985; 92:741–748. [PubMed: 4034169]

43. Ravi S, Haller CA, Sallach RE, Chaikof EL. Cell behavior on a CCN1 functionalized elastin-mimetic protein polymer. Biomaterials. 2012; 33:2431–2438. [PubMed: 22212194]

44. Zorlutuna P, Elsheikh A, Hasirci V. Nanopatterning of collagen scaffolds improve the mechanical properties of tissue engineered vascular grafts. Biomacromolecules. 2009; 10:814–821. [PubMed: 19226102]

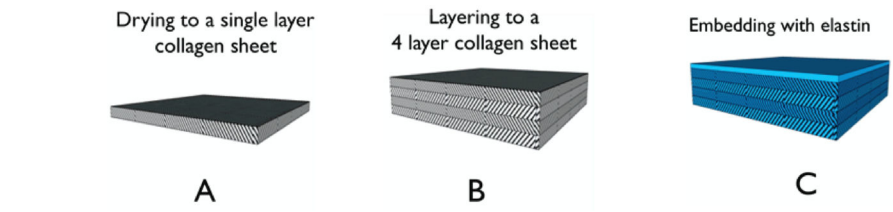

Figure 1.

Schematic of fabrication strategy for layered collagen elastin hybrids. Collagen gels were cast at 4 mm thickness. (A) Collagen lamellae were dried to a dry thickness of approximately 35 μm, (B) and layered into *multi-layer* collagen mats and ablated. (C) Multilayer lamellae were embedded with elastin (blue) into a multi-layer hybrid.

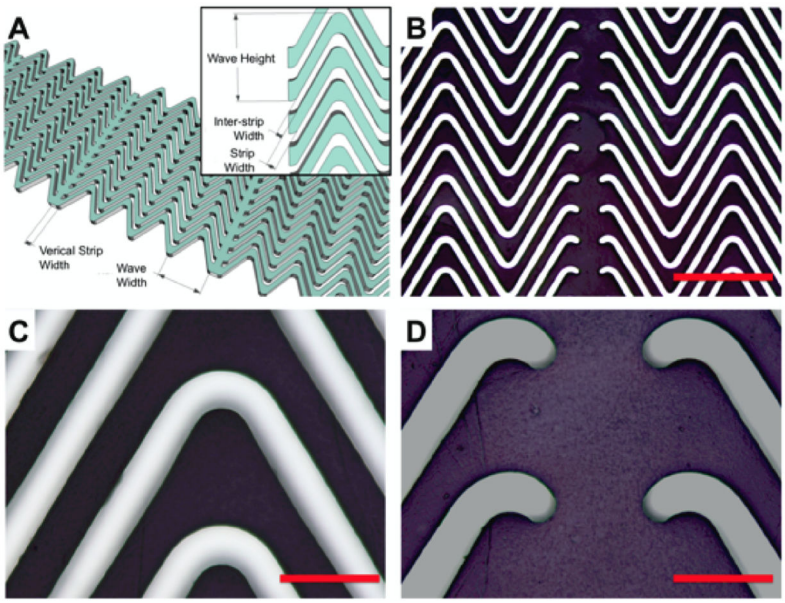

Figure 2.

Ablation schemes of collagen mats. (A) Schematic of collagen lamella ablated using an excimer laser to create a defined “wavy” collagen lamella with linear supports, inset shows additional nomenclature. (B) Uniformity and transfer of wavy ablated pattern with high fidelity onto collagen mats, scale bar 500 μm. (C-D) Ablated collagen lamella displayed clear excimer laser cuts with no apparent material damage, scale bar 100 μm.

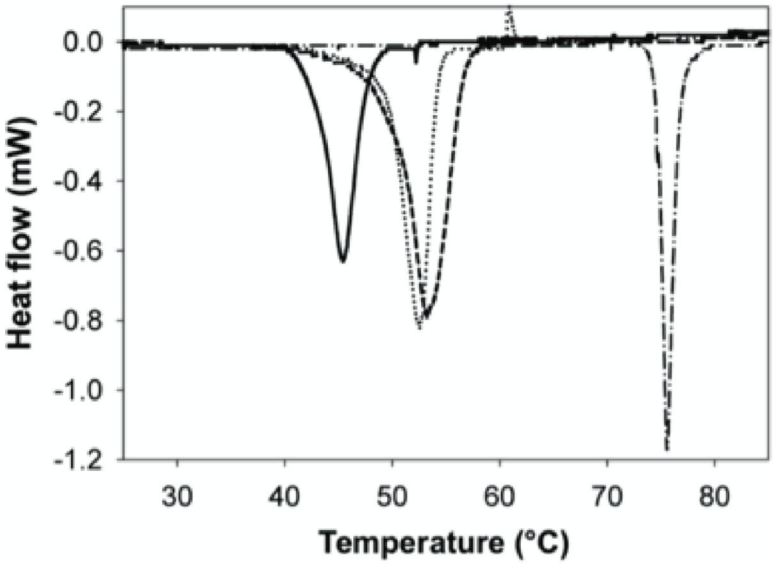

Figure 3.

Endothermic heat transitions of collagen mats. Microdifferential scanning calorimetry of lyophilized collagen (solid), collagen lamella (dotted), excimer ablated collagen film (dash), genipin crosslinked collagen lamella (dash-dot). (n = 3)

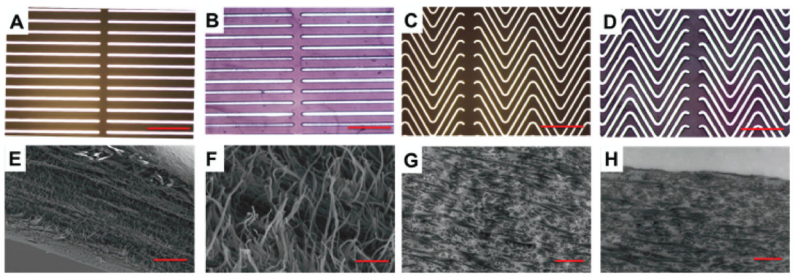

Figure 4.

Meso- and ultra-structure of collagen mats of varying vertical strip width. (A & C) Optical micrographs of aluminum-on-quartz masks, scale bar 500 μm. (B & D) Optical micrographs of genipin crosslinked collagen lamellae, scale bar 500 μm. SEM of wavy collagen mats (E) wave edge 5 kX, and (F) magnified view of fibrillar structure 50 kX, scale bars 10 μm, 1 μm respectively. TEM images of wavy collagen mats, (G) 10 kX bulk and (H) 10 kX wave edge, scale bar 1 μm.

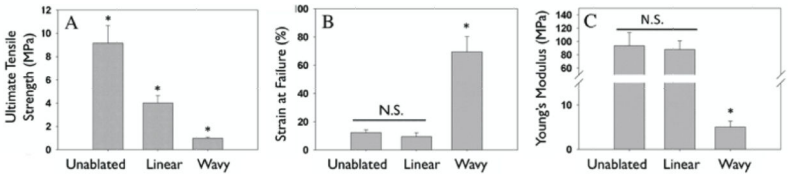

Figure 5.

Mechanical properties of collagen-elastin hybrids. A: Ablation of collagen with linear and wavy pattern resulted in a significant decrease in ultimate tensile strength (A) of hybrids. Strain at failure for unablated and linear ablated collagen-elastin hybrids did not change significantly, however, introduction of waveform pattern significantly increased strain at failure. Stiffness did not change significantly for unablated or linear ablated hybrids, but significantly decreased for wavy hybrids. (*$p < 0.05$)

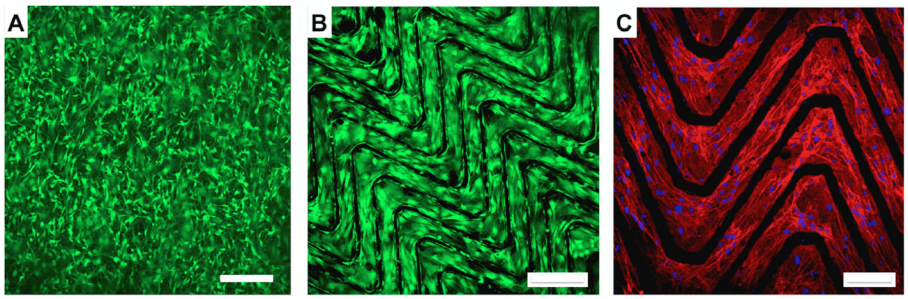

Figure 6.

Cellularization of unablated and ablated hybrid scaffolds. (A)Unablated scaffold seeded with rMSCs at 100,000 cells/cm^2, for 24 h Live (green)/Dead (red) stained. (B) Ablated scaffold seeded with rMSCs at 100,000 cells/cm^2, for 24 h. (C) Actin cytoskeletal staining and DAPI nuclei staining showing cells conforming to ablated scaffolds. Scale bar: A & B: 250 μm, C: 100 μm.

Table 1

Thermal properties of collagen mat

	Monomeric collagen*	Lyophilized collagen	Collagen mat	Excimer-treated collagen mat	Genipin crosslinked collagen mat
T_D (°C)	36.2 ± 0.6	46.0 ± 0.5	52.9 ± 0.3	53.1 ± 0.20	73.2 ± 2.1
ΔH (J/g)	49.4 ± 0.8	47.8 ± 4.7	44.0 ± 3.2	48.2 ± 1.32	27.3 ± 1.8

* adapted from Caves et al [7].

Table 2

Mechanical properties of unablated and ablated collagen-elastin hybrids.

	Ultimate Tensile Strength (MPa)	Strain at Failure (%)	Young's Modulus (MPa)
Unablated hybrids	13.0 ± 2.1	18.0 ± 3.7	93 ± 20
Ablated hybrids	0.7 - 5.8	9.4 - 70	2.9 - 88
Blood vessels*	1.0 - 11	40 - 100	1.0 – 2.0
Cartilage & Ligament*	3 - 110	10 - 120	0.7 - 500

* average values from [8, 19, 25, 26].